# Supporting Information

## Yamashita et al. 10.1073/pnas.1110402108

### SI Discussion

**Mechanism for Controlling Fidelity of Oligomerization.** We have demonstrated that incorrect homodimers are never formed in the dimerization step (1, 2). If two identical molecules associate into a dimer, electrostatic repulsion will occur between the residues, forming interprotomer ion pairs in the cap—rim interface (Fig. 2*B*). These residues would contribute to the fidelity control of multimerization by obstructing homodimer formation as well as stabilization of the interprotomer interaction.

In the structure model of prepore, the steric restraint at interface 2 covered a wider range than that at interface 1 (Fig. S4*B*), suggesting that energy required for the conformation change of the amino-latch and prestem at interface 2 is larger than that of interface 1. The difference may also be a determinant for the priority of dimerization.

**Functions of Individual Molecules in Pore Formation.** Biochemical data and the present octameric pore structure clearly showed that LukF is important for binding to the cell surface and is responsible for the structural transition from prepore to pore (1, 3). In contrast, the role of Hlg2 is obscure, although it was demonstrated that Hlg2 recognizes proteinaceous factor(s) located at the erythrocyte surface (4). In the present study, octameric pores were formed by 2-methyl-2,4-pentanediol (MPD) without membranes, suggesting that neither pore formation nor oligomerization require contact with the membrane. Crystallization was performed at extremely high protein concentration in comparison with biochemical assays, suggesting that γ-hemolysin (γ-HL) can form a pore structure spontaneously if the concentration is sufficiently high and the lipid head group or MPD is captured by Trp177 of LukF. In the previous biochemical assay, γ-HL could form a pore on an artificial membrane not containing the receptor molecule of Hlg2, although it required an approximately 100-fold higher concentration than for that on erythrocytes (5). Under these conditions, γ-HL probably forms pores due to the property of spontaneous assembly at high concentration. On the other hand, only about 10,000 molecules each of the γ-HL component (which forms 2,500 octameric pores) are sufficient for complete hemolysis of a human erythrocyte (4). Assuming that this amount of each molecule is distributed evenly on the erythrocyte surface, the density of the toxin components is expected to be very low for prepore formation. Hlg2 may contribute to effective condensation of heterodimers on the cell surface through binding with its receptor molecule(s). In fact, leukocidin forms pores on lipid rafts of leukocyte membranes (6). Taken together, it is reasonable to propose that components of γ-HL share roles in pore formation as follows; LukF is responsible for initial cell binding and induction of the structural change from prestem to stem, whereas Hlg2 acts to increase the local concentration of heterodimers by capturing receptor molecules.

### SI Methods

**Preparation of LukF and Hlg2.** Two different DNA fragments encoding LukF and Hlg2 without the signal sequence were amplified using KOD-Plus DNA polymerase (Toyobo), and inserted into the *Nco*I and *Xho*I sites of the pET26 vector (Merck). A His6-tag was fused at the N terminus to facilitate purification. Transformed *Escherichia coli* strain B834(DE3) harboring the expression vector of the desired protein and pRAREII (Merck) was grown at 37 °C in LB medium supplemented with 25 μg mL$^{-1}$ kanamycin and 34 μg mL$^{-1}$ chloramphenicol until the logarithmic growth phase. To induce expression of the desired protein, isopropyl-β-D-thiogalactopyranoside was added to a final concentration of 0.5 mM, and culture was continued for 18 h at 25 °C. Cells were harvested by centrifugation at 4,500 × *g* for 10 min at 4 °C, and then disrupted using a sonicator (Branson) in 20 mM Tris-HCl (pH 8.0), 300 mM NaCl. The cell debris was removed by centrifugation at 40,000 × *g* for 1 h at 10 °C, and the supernatant was loaded onto a Ni sepharose 6 Fast Flow column (GE Healthcare Biosciences AB). After washing with the same buffer, the adsorbed protein was eluted with a gradient of imidazole. Fractions containing the desired protein were further purified on a HiLoad 26/60 Superdex 200-pg column (GE Healthcare Biosciences AB). Purified monomeric proteins were stored at 4 °C until use.

**Crystallization and X-Ray Diffraction Data Collection.** The 1:1 mixtures of LukF and Hlg2 monomers were concentrated to 4 mg mL$^{-1}$. Crystals suitable for further experiments were grown by the sitting-drop vapor diffusion method from a solution containing 0.1 M sodium acetate (pH 4.6), 0.5 M ammonium acetate, and 50% (v/v) MPD. X-ray diffraction experiments were performed on the beamline BL41XU at SPring-8. The γ-hemolysin crystal belonged to space group $C222_1$ with unit cell parameters $a = 206.45$ Å, $b = 206.14$ Å, $c = 190.30$ Å. Diffraction data were indexed, integrated, scaled, and merged with the program XDS (7). This crystal was pseudomerohedrally twinned with twin operator $(-k, -h, -l)$ and the twin fraction was estimated as 42% by Britton analysis performed with the program phenix.xtriage (8). It should be noted that the apparent lattice symmetry was tetragonal; however, in such a space group, the resultant model from molecular replacement clashed with its symmetry mates. *R* vs. *R* statistics (9) indicated that the crystal was pseudomerohedrally twinned with rotational pseudosymmetry. Data collection statistics are shown in Table 2.

The structure of γ-hemolysin was determined by the molecular replacement method with the program Phaser (10) using the structures of monomeric LukF [Protein Data Bank (PDB) ID code 1lkf (11), Hlg2 [PDB ID code 2qk7 (12)], and the stem region of α-hemolysin protomer [PDB ID code 3anz (13)] as search probes. The prestem regions of LukF and Hlg2 were removed before molecular replacement. Molecular replacement resulted in the octameric complex in the asymmetric unit. To monitor the refinement, a random 3.0% subset from all unique reflections was set aside for *R*-free evaluation, taking lattice symmetry into account with the program phenix.reflection_file_editor (8). Jelly body refinement with local NCS restraints was performed with the program REFMAC5 (14) after rigid body refinement. After several cycles of manual model fitting and building with Coot (15) and refinement with REFMAC5, individual atomic coordinate refinement and individual ADP refinement were performed with phenix.refine (8). The twin operator $(k, h, -l)$ was applied during every round of refinement and the twin fraction was refined. Finally, *R*-work and *R*-free values converged to 20.68% and 23.64%, respectively. The stereochemical qualities of the final refined model were analyzed with phenix.validate including MolProbity analysis (16). The buried surface area was calculated with the program PISA (17). The number of atoms participating in interprotomer van der Waals interaction and interprotomer polar interaction were calculated with the program CONTACT and PISA in the ccp4 program package (18), respectively. The refinement statistics are summarized in Table S2.

1. Nguyen VT, Kamio Y, Higuchi H (2003) Single-molecule imaging of cooperative assembly of gamma-hemolysin on erythrocyte membranes. *EMBO J* 22:4968–4979.
2. Nguyen AH, Nguyen VT, Kamio Y, Higuchi H (2006) Single-molecule visualization of environment-sensitive fluorophores inserted into cell membranes by staphylococcal gamma-hemolysin. *Biochemistry* 45:2570–2576.
3. Ozawa T, Kaneko J, Kamio Y (1995) Essential binding of LukF of staphylococcal gamma-hemolysin followed by the binding of H gamma II for the hemolysis of human erythrocytes. *Biosci Biotechnol Biochem* 59:1181–1183.
4. Kaneko J, Ozawa T, Tomita T, Kamio Y (1997) Sequential binding of Staphylococcal gamma-hemolysin to human erythrocytes and complex formation of the hemolysin on the cell surface. *Biosci Biotechnol Biochem* 61:846–851.
5. Ferreras M, et al. (1998) The interaction of Staphylococcus aureus bicomponent gamma-hemolysins and leucocidins with cells and lipid membranes. *Biochim Biophys Acta* 1414:108–126.
6. Nishiyama A, Kaneko J, Harata M, Kamio Y (2006) Assembly of staphylococcal leukocidin into a pore-forming oligomer on detergent-resistant membrane microdomains, lipid rafts, in human polymorphonuclear leukocytes. *Biosci Biotechnol Biochem* 70:1300–1307.
7. Kabsch W (2010) XDS. *Acta Crystallogr D Biol Crystallogr* 66:125–132.
8. Adams PD, et al. (2010) PHENIX: a comprehensive Python-based system for macromolecular structure solution. *Acta Crystallogr D Biol Crystallogr* 66:213–221.
9. Lebedev AA, Vagin AA, Murshudov GN (2006) Intensity statistics in twinned crystals with examples from the PDB. *Acta Crystallogr D Biol Crystallogr* 62:83–95.
10. McCoy AJ, et al. (2007) Phaser crystallographic software. *J Appl Crystallogr* 40:658–674.
11. Olson R, Nariya H, Yokota K, Kamio Y, Gouaux E (1999) Crystal structure of staphylococcal LukF delineates conformational changes accompanying formation of a transmembrane channel. *Nat Struct Biol* 6:134–140.
12. Roblin P, et al. (2008) A covalent S-F heterodimer of leucotoxin reveals molecular plasticity of β-barrel pore-forming toxins. *Proteins* 71:485–496.
13. Tanaka Y, et al. (2011) 2-Methyl-2,4-pentanediol induces spontaneous assembly of staphylococcal α-hemolysin into heptameric pore structure. *Protein Sci* 20:448–456.
14. Murshudov GN, et al. (2011) REFMAC5 for the refinement of macromolecular crystal structures. *Acta Crystallogr D Biol Crystallogr* 67:355–367.
15. Emsley P, Lohkamp B, Scott WG, Cowtan K (2010) Features and development of Coot. *Acta Crystallogr D Biol Crystallogr* 66:486–501.
16. Chen VB, et al. (2010) MolProbity: all-atom structure validation for macromolecular crystallography. *Acta Crystallogr D Biol Crystallogr* 66:12–21.
17. Krissinel E, Henrick K (2007) Inference of macromolecular assemblies from crystalline state. *J Mol Biol* 372:774–797.
18. Collaborative Computational Project, Number 4(1994) The CCP4 suite: Programs for protein crystallography. *Acta Crystallogr D Biol Crystallogr* 50:760–763.

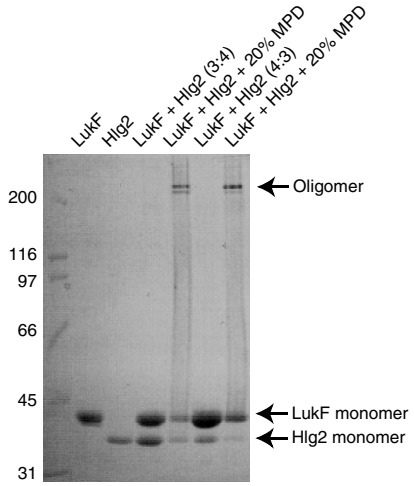


**Fig. S1.** Oligomer formation by MPD. Purified monomeric LukF and Hlg2 were incubated with or without MPD. Oligomer formation was confirmed by SDS-PAGE. SDS-resistant hetero-oligomer was formed with 20% MPD.

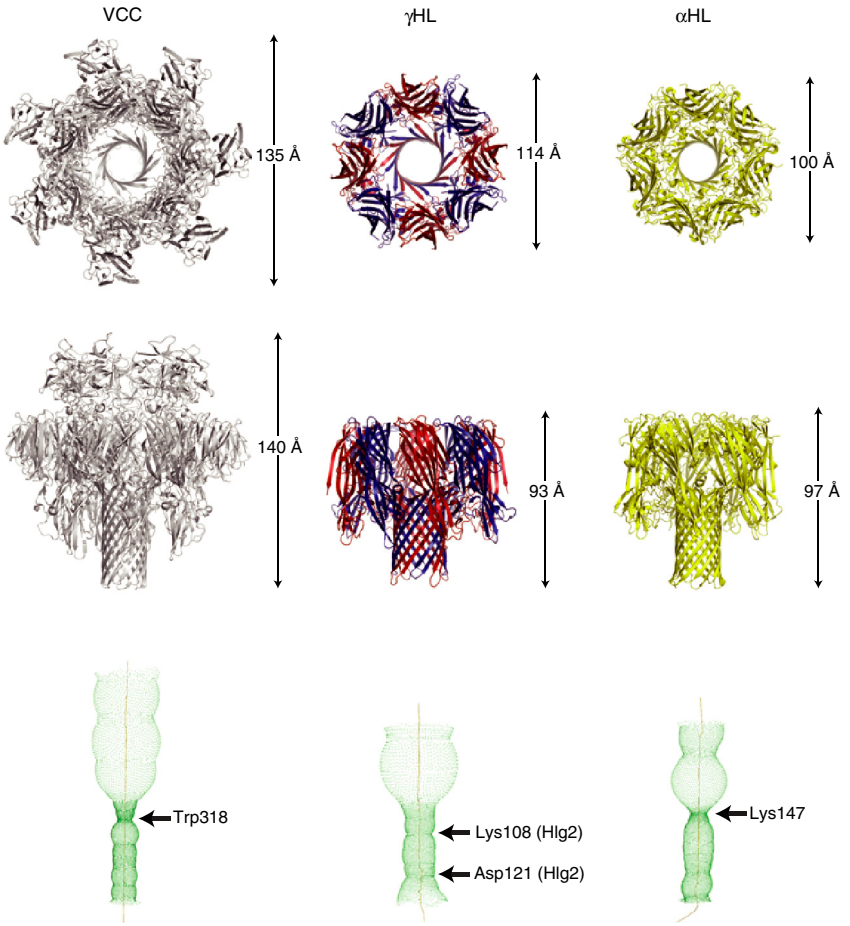


**Fig. S2.** Comparison of the pore structures among γHL (*Center*), *Vibrio cholerae* (VCC) (*Left*), and α-helical pore-forming toxin (PFT) (αHL) (*Right*). Diameter and height are indicated. The bottom figures show the outline of the central vestibule and channel of pores calculated using the program HOLE (1). Constriction and the residues responsible are also indicated. The central axis is shown as a yellow line.

1 Smart OS, Goodfellow JM, Wallace BA (1993) The pore dimensions of gramicidin A. *Biophys J* 65:2455–2460.

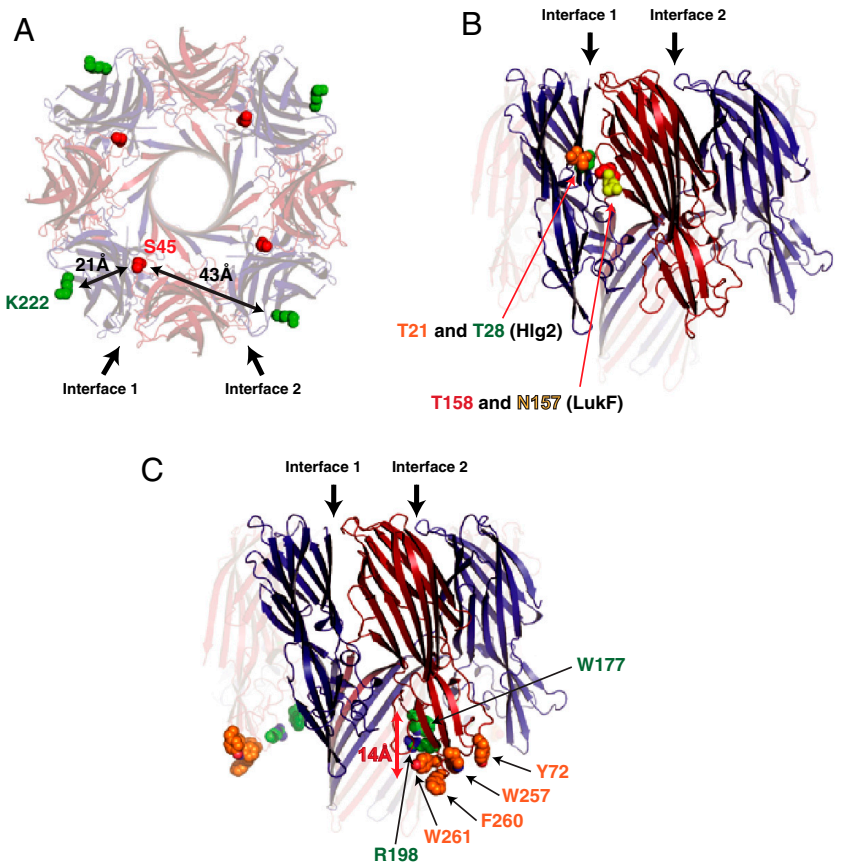


**Fig. S3.** Residues mentioned in *Discussion*. (*A*) Lys222 of Hlg2 (green) and Ser46 of LukF (red) are shown as spheres. In the study reported by Nguyen et al. (1), TMR and IC5 were introduced into these residues for the FRET experiment. The distance between these residues in the dimer through interface 1 is 21 Å, whereas that though interface 2 is 43 Å. Upon dimer, tetramer, hexameric assembly, the FRET intensity increased proportionally (1), showing that the initial heterodimer is formed through interface 1. (*B*) Thr28 (orange) and Thr21 (green) of Hlg2, and Asn157 (red) and Thr158 (yellow) of LukF are shown as spheres. In the study reported by Joubert et al. (2), Thr28 (Hlg2)—Asn157 (LukF), and Thr21 (Hlg2)—Thr158 (LukF) were covalently linked. These mutants could effectively form pores. (*C*) Tyr72, Trp257, Phe260, and Tyr261 of LukF, necessary for the initial cell binding (3–5), are shown as orange spheres. The phospholipid head group binding residues, Trp177 and Arg198, are also shown as green spheres (6). The vertical interval between Phe260 and Trp177 was 14 Å, suggesting the inclining orientation of LukF upon attachment to the cell surface.


1 Nguyen VT, Kamio Y, Higuchi H (2003) Single-molecule imaging of cooperative assembly of gamma-hemolysin on erythrocyte membranes. *EMBO J* 22:4968–4979.
2 Joubert O, et al. (2006) Engineered covalent leucotoxin heterodimers form functional pores: Insights into S–F interactions. *Biochem J* 369:381–389.
3 Monma N, Nguyen VT, Kaneko J, Higuchi H, Kamio Y (2004) Essential residues, W177 and R198, of LukF for phosphatidylcholine-binding and pore-formation by staphylococcal gamma-hemolysin on human erythrocyte membranes. *J Biochem* 136:427–431.
4 Yokota K, Kamio Y (2000) Tyrosine72 residue at the bottom of rim domain in LukF crucial for the sequential binding of the staphylococcal gamma-hemolysin to human erythrocytes. *Biosci Biotechnol Biochem* 64:2744–2747.
5 Nguyen VT, Kamio Y (2004) Cooperative assembly of beta-barrel pore-forming toxins. *J Biochem* 136:563–567.
6 Olson R, Nariya H, Yokota K, Kamio Y, Gouaux E (1999) Crystal structure of staphylococcal LukF delineates conformational changes accompanying formation of a transmembrane channel. *Nat Struct Biol* 6:134–140.

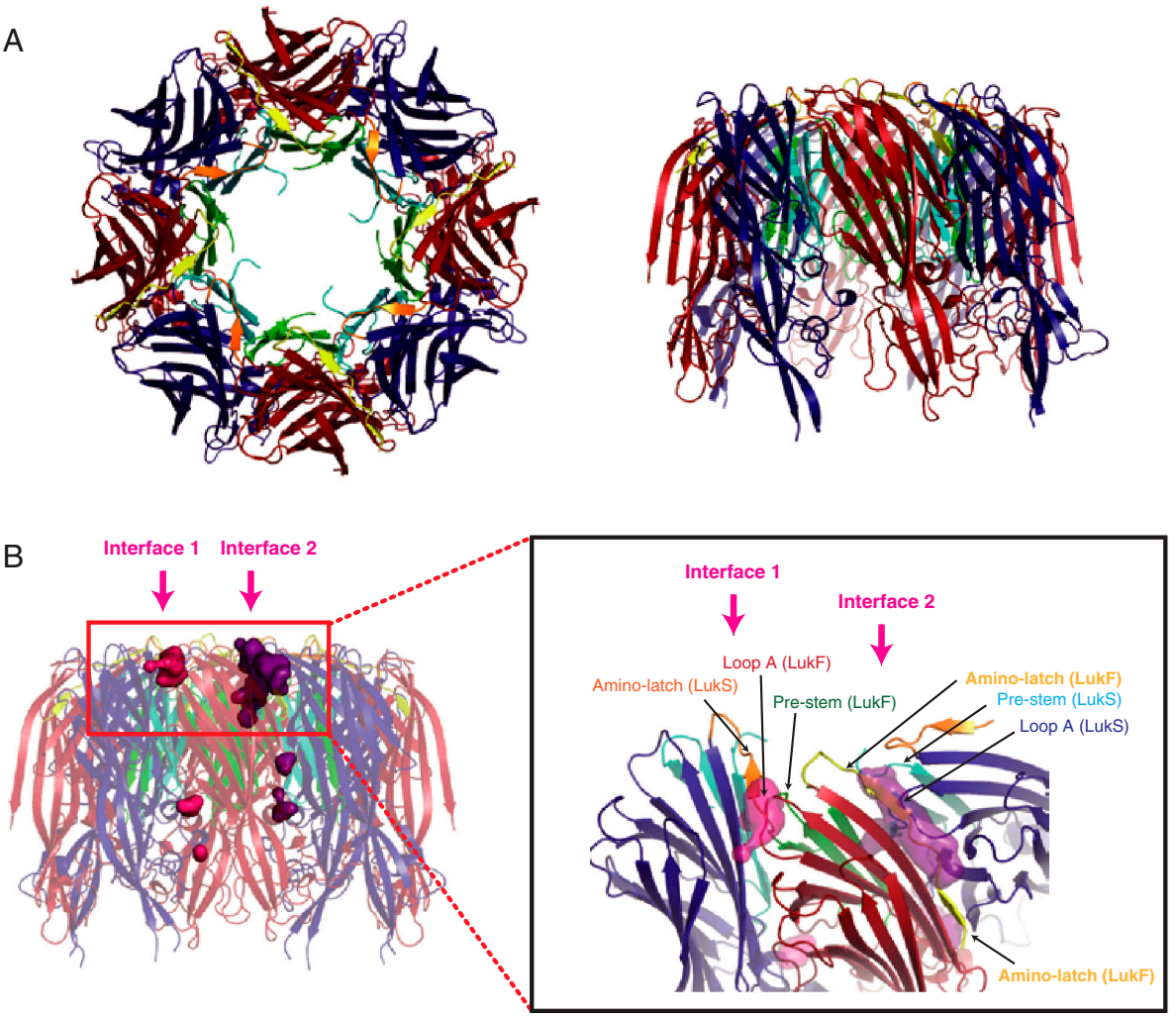


**Fig. S4.** Prepore model. (*A*) Top and side view of the prepore structure constructed by superposing monomeric LukF and LukS onto protomers of LukF and Hlg2, respectively. As the amino-latch was not constructed in the crystal structure of monomeric Hlg2, LukS monomer was used as the S-component. Red, cap and rim domains of LukF; blue, those of LukS; green, prestem of LukF; cyan, that of LukS; yellow, amino-latch of LukF; orange, that of LukS. (*B*) Steric collisions between protomers. Clashing atoms at interfaces 1 and 2 are shown as magenta and purple surfaces, respectively. Close-up view around the top of the interfaces is also shown. Colors in the cartoon correspond to those in Fig. S4*A*.

**Table S1. Observed interprotomer interactions**

| Interface | | | Number of atoms participating in the interprotomer interaction | | | |
|---|---|---|---|---|---|---|
| | | | van der Waals interaction | | Polar interaction | |
| Interface 1 | | | | | | |
| | LukF | Hlg2 | LukF | Hlg2 | LukF | Hlg2 |
| | cap | cap | 177 | 169 | 38 | 46 |
| | cap | rim | 66 | 94 | 24 | 23 |
| | cap | stem | 0 | 0 | 0 | 0 |
| | cap | triangle loop | 0 | 0 | 0 | 0 |
| | rim | cap | 0 | 0 | 0 | 0 |
| | rim | rim | 59 | 38 | 7 | 7 |
| | rim | stem | 0 | 0 | 0 | 0 |
| | rim | triangle loop | 0 | 0 | 0 | 0 |
| | stem | cap | 0 | 0 | 0 | 0 |
| | stem | rim | 56 | 40 | 8 | 8 |
| | stem | stem | 290 | 298 | 87 | 95 |
| | stem | triangle loop | 0 | 0 | 0 | 0 |
| | triangle loop | cap | 48 | 49 | 16 | 16 |
| | triangle loop | rim | 22 | 25 | 4 | 4 |
| | triangle loop | stem | 4 | 10 | 0 | 0 |
| | triangle loop | triangle loop | 28 | 24 | 6 | 6 |
| | total* | | 750 (460) | 747 (449) | 190 (103) | 205 (110) |
| Interface 2 | | | | | | |
| | LukF | Hlg2 | LukF | Hlg2 | LukF | Hlg2 |
| | cap | cap | 219 | 205 | 59 | 49 |
| | cap | rim | 0 | 0 | 0 | 0 |
| | cap | stem | 0 | 0 | 0 | 0 |
| | cap | triangle loop | 41 | 40 | 12 | 8 |
| | rim | cap | 16 | 16 | 8 | 8 |
| | rim | rim | 24 | 36 | 3 | 3 |
| | rim | stem | 11 | 6 | 1 | 1 |
| | rim | triangle loop | 8 | 22 | 0 | 0 |
| | stem | cap | 0 | 0 | 0 | 0 |
| | stem | rim | 0 | 0 | 0 | 0 |
| | stem | stem | 291 | 277 | 78 | 78 |
| | stem | triangle loop | 8 | 4 | 0 | 0 |
| | triangle loop | cap | 0 | 0 | 0 | 0 |
| | triangle loop | rim | 0 | 0 | 0 | 0 |
| | triangle loop | stem | 0 | 0 | 0 | 0 |
| | triangle loop | triangle loop | 16 | 21 | 4 | 8 |
| | total* | | 634 (343) | 627 (350) | 165 (87) | 155 (77) |

*The values in parentheses refer to total number except stem–stem interaction.

**Table S2. Data collection and refinement statistics**

| | |
|---|---|
| Data collection | |
| Beamline | SPring-8 BL41XU |
| Detector | Rayonix MX225HE |
| Wavelength (Å) | 1.00000 |
| Space group | $C222_1$ |
| Cell dimensions (Å) | $a = 206.45$, $b = 206.14$, $c = 190.30$ |
| Resolution range (Å) * | 43.30-2.49 (2.65-2.49) |
| $R_{sym}$ (%) * | 11.1 (65.1) |
| $\langle I/\sigma(I)\rangle$ * | 14.3 (3.5) |
| Completeness (%) * | 98.9 (96.3) |
| Multiplicity * | 7.6 (6.8) |
| No. of observed reflections * | 1,054,332 (147,704) |
| No. of unique reflections * | 138,838 (21,660) |
| Refinement | |
| Resolution (Å) | 43.30-2.49 |
| *R*-work (%) | 20.68 |
| *R*-free (%) | 23.64 |
| Twin fraction (%) | 44.3 ($-k$, $-h$, $-l$) |
| $R_{twin,obs}$, $R_{twin,calc}$ (%) † | 6.5, 43.4 |
| No. of protein atoms | 17,896 |
| No. of ligand atoms | 32 |
| No. of water molecules | 449 |
| Average B-factors (Å$^2$) | |
| protein atoms | 43.78 |
| ligand atoms | 70.40 |
| water molecules | 31.30 |
| rmsd from ideal | |
| bond lengths (Å) | 0.009 |
| bond angles (°) | 1.125 |
| Ramachandran plot ‡ | |
| residues in favored region | 2,136 (97.1%) |
| residues in allowed region | 64 (2.9%) |
| residues in outlier region | 0 (0.0%) |

*The values in parentheses refer to data in the highest resolution shell.

†$R_{twin} = \Sigma|I(\boldsymbol{h}) - I(S_{twin}\boldsymbol{h})|/\Sigma(I(\boldsymbol{h}) + I(S_{twin}\boldsymbol{h}))$, where $S_{twin}$ is the twin operator (1).

‡Ramachandran plot analyses were performed using *RAMPAGE* (2).

1 Lebedev AA, Vagin AA, Murshudov GN (2006) Intensity statistics in twinned crystals with examples from the PDB.*Acta Crystallogr D Biol Crystallogr* 62:83–95.
2 Lovell SC, et al. (2003) Structure validation by Calpha geometry: Phi, psi and Cbeta deviation.*Proteins* 50:437–450.